JOURNAL OF CHEMICAL INFORMATION AND MODELING

Article

pubs.acs.org/jcim

# Influence of Protonation on Substrate and Inhibitor Interactions at the Active Site of Human Monoamine Oxidase-A

Gerald Zapata-Torres,*[,†] Angelica Fierro,[‡] Sebastian Miranda-Rojas,[†] Carlos Guajardo,[‡] Patricio Saez-Briones,[§] J. Cristian Salgado,[∥] and Cristian Celis-Barros[†]

[†]Molecular Graphics Suite, Department of Inorganic and Analytical Chemistry, Faculty of Chemical and Pharmaceutical Sciences, University of Chile, Santiago, Chile

[‡]Department of Organic Chemistry, Faculty of Chemistry, Pontificia Universidad Católica de Chile, Santiago, Chile

[§]School of Medicine, Faculty of Medical Sciences, University of Santiago de Chile, Santiago, Chile

[∥]Laboratory of Process Modeling and Distributed Computing, Department of Chemical Engineering and Biotechnology, University of Chile, Santiago, Chile

Supporting Information

**ABSTRACT:** Although substrate conversion mediated by human monoaminooxidase (hMAO) has been associated with the deprotonated state of their amine moiety, data regarding the influence of protonation on substrate binding at the active site are scarce. Thus, in order to assess protonation influence, steered molecular dynamics (SMD) runs were carried out. These simulations revealed that the protonated form of the substrate serotonin (5-HT) exhibited stronger interactions at the protein surface compared to the neutral form. The latter displayed stronger interactions in the active site cavity. These observations support the possible role of the deprotonated form in substrate conversion. Multigrid docking studies carried out to rationalize the role of 5-HT protonation in other sites besides the active site indicated two energetically favored docking sites for the protonated form of 5-HT on the enzyme surface. These sites seem to be interconnected with the substrate/inhibitor cavity, as revealed by the tunnels observed by means of CAVER program. p$K_a$ calculations in the surface loci pointed to Glu[327], Asp[328], His[488], and Asp[132] as candidates for a possible in situ deprotonation step. Docking analysis of a group of inhibitors (structurally related to substrates) showed further interactions with the same two docking access sites. Interestingly, the protonated/deprotonated amine moiety of almost all compounds attained different docking poses in the active site, none of them oriented to the flavin moiety, thus producing a more variable and less productive orientations to act as substrates. Our results highlight the role of deprotonation in facilitating substrate conversion and also might reflect the necessity of inhibitor molecules to adopt specific orientations to achieve enzyme inhibition.

## INTRODUCTION

Monoaminooxidase (MAO) is a flavin adenine dinucleotide (FAD)-containing enzyme that exists in two isoforms (MAO-A and MAO-B), and it is essential for the metabolism of amine neurotransmitters with different specificities, with serotonin (5-HT) being a preferred MAO-A substrate.[1] Because of its pharmacological relevance, several inhibitors (MAOi) that differ in potencies and selectivities have been developed as tools for the treatment of several psychiatric and neurological disorders.[2−4] In this regard, (MAOi)-As have been used as antidepressant and/or anxiolytic drugs,[1−5] whereas (MAOi)-Bs have been used as adjuvant in the treatment of neurodegenerative disorders, such as Parkinson disease.[6] Among the (MAOi)-As already studied, those with closely structural similarities to endogenous substrates are of particular interest, as is the case of amphetamine-based inhibitors.[2] Structural modifications of these compounds so far have included substitutions on the amine nitrogen, $\alpha$-alkylation, and $\beta$-oxygenation of the ethyl side chain, as well as different substitutions at the aromatic ring, including extension of the $\pi$ system (Figure 1). Several of these compounds, particularly $\alpha$-methylphenylethylamines with a single alkoxy or alkylthio substituent at the *para* position, have been proved to be active as (MAOi)-As with negligible (MAOi)-Bs activity.[7]

At a standard physiological pH, primary biogenic amines and alkylphenylisopropylamine inhibitors are expected to exist as protonated species; an assumption that is compatible with the acid dissociation constant calculated for serotonin (5-HT) (p$K_a$ = 9.97).[8] Nevertheless, the experimental evidence regarding the protonation state (i.e., charged or uncharged species) for substrates and/or inhibitors upon binding to human MAO-A (hMAO-A) is scarce and in disagreement.[9,10] Jones et al.[9] concluded that uncharged inhibitors bind hMAO-A better, but the predominant species of the amine in the pH range of 7−9 is protonated and therefore must be the substrate. In contrast, Dunn et al.[10] concluded from kinetic isotope and pH studies

**Received:** February 8, 2012
**Published:** April 29, 2012





dx.doi.org/10.1021/ci300081w | *J. Chem. Inf. Model.* 2012, 52, 1213−1221

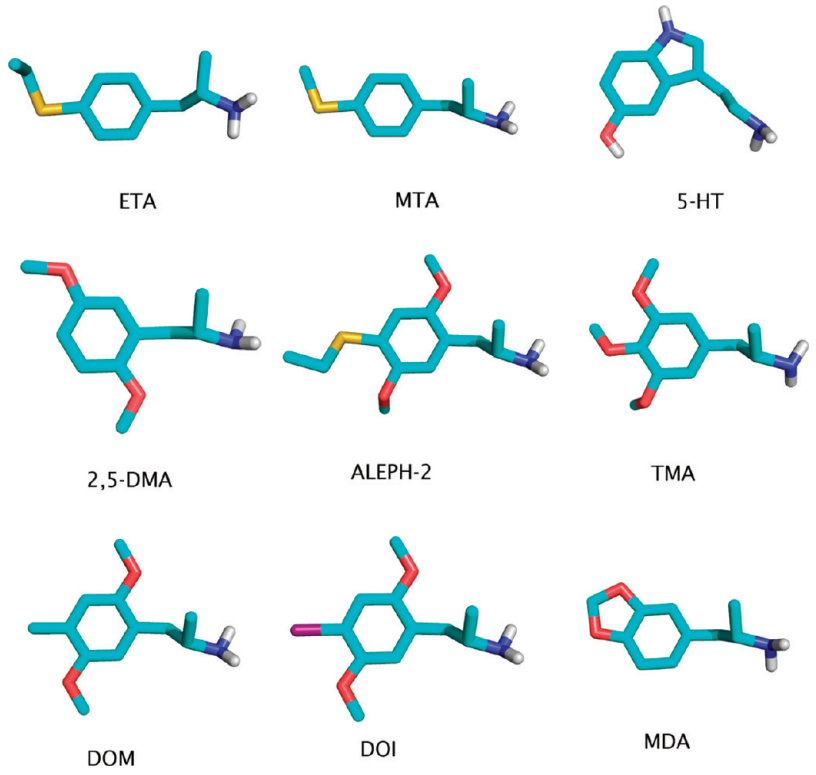


**Figure 1.** Monoamine oxidase A serotonin (5-HT) and phenylispropylamines inhibitors. PyMol (www.pymol.org) was used for the preparation of all structures figures.

with hMAO-A that deprotonation of the amine is required for catalysis.

Moreover, the currently proposed mechanisms for substrate conversion consider catalysis initiation as the result of the interaction of a deprotonated substrate with the isoalloxazine moeity to create the enzyme–substrate complex.[9] This still unsolved issue prompted us to hypothesize about a possible in situ deprotonation process by specific amino acids belonging to the enzyme's surface, which should occur prior to substrate oxidation and/or enzyme inhibition occurrence, taking into account that there are no negatively charged or basic residues in the enzyme active site or entrance cavity.

Interestingly, regardless of the numerous molecules studied, there are no efforts focused on elucidating the structural requirements that govern the access of substrates or inhibitors to the active site from the putative entrance cavity. In fact, in spite of the several crystal structures published[11,12] and docking studies carried out,[13,14] none of them has led to the understanding of those relevant events.

In the present work, we used molecular modeling studies, including steered molecular dynamics, flexible molecular multigrid docking, and p$K_a$ calculations, to address these issues. Our results shed light on the possible role of the protonation/deprotonation process of 5-HT on the translation from the entrance to the catalytic site. Also, the results allow us to propose residues candidates located on the enzyme surface responsible of this deprotonation step. The docking of some amphetamine-based inhibitors (hMAO-Ai) revealed interactions in the same two docking sites previously identified for protonated 5-HT. The interactions observed on the active site allow us to describe key interactions associated with possible ligand conformational changes that might be required for productive orientations within the active site.

## METHODS

**Protonation State of Titrable Residues.** The X-ray crystal structure of hMAO-A was taken from the Protein Databank (PDB code 2Z5X).[11] In order to add hydrogen atoms to this structure, the protonation states of titrable amino-acids were defined at pH 7.4 using the H++ server that implements a Poisson–Boltzmann method calculation.[15]

**Quantum Mechanical Calculations.** Full geometry optimization of substrate (5-HT) and all inhibitors (Figure 1) for docking studies were performed at the B3LYP/6-31G(d,p) level of theory using the Gaussian 98 package.[16] Neutral and protonated forms for substrate and inhibitors were included because their alkylamine side chain should be protonated at physiological pH.

**Multigrid Procedure.** In order to investigate possible docking sites on the surface, the whole enzyme surface was examined using several grids. The enzyme was set at the origin of the Cartesian coordinates, and it was aligned along the *z*-axis. Then a grid box with a size of 70 × 70 × 70 points with spacing of 0.375 Å was set up at a corner of the enzyme. Subsequently, a series of grid boxes were defined along the *x*-axis until a box was finally located at the opposite side of the enzyme. A displacement of 14 Å along the *x*-axis was chosen in order to overlap the grids. Once the boxes were all set in the *x*-axis, a new set of grids along the *y*-axis were generated from each box aligned over the *x*-axis. Similarly, from the rectangular set of grid boxes covering the *x*–*y* plane at the edge of the enzyme, a new set of boxes were generated along the *z*-axis from each one of the previously defined grids. Using this procedure, the whole enzyme was completely enclosed by the grid boxes.

**Multigrid Docking Calculations.** On the basis of the already obtained grid boxes, a multigrid docking of substrate and inhibitors in the surface and into the active site of the

crystal structure of h-MAO-A was performed with the AutoDock 3.0.5 package,[17] using the Lamarckian algorithm and total flexibility for substrate and inhibitors: population size, 150; number of evaluations, $1.5 \times 10^6$; number of generations, $1.5 \times 10^5$; mutation rate, 0.2; crossover rate, 0.8; and number of runs, 200. The AutoTors option was used to define the ligand torsions. Docking results were analyzed by a ranked cluster procedure, resulting in conformations with the lowest overall binding energy.

**Molecular Dynamics Simulations.** All energy minimizations, molecular dynamics simulations in order to make the enzyme−ligand complex reach its thermodynamic equilibration states, and Steered Molecular Dynamic (SMD) were carried out with NAMD 2.6.[18] CHARMM27 force field parameters[19,20] for the protein and gaff parameters[21] for the substrate were used.

The protein was inserted in a phospholipid bilayer (POPC) using the CHARMM27 force field for phospholipids. The system was fully solvated in a TIP3 water box of 120 Å$^3$ and neutralized in 0.02 M NaCl.

The whole MD simulation procedure comprised two minimizations and three MD simulation runs, as described below.

(1) The whole system was minimized (1000 steps) followed by a MD for lipid tail accommodation (250,000 steps). (2) A second minimization was carried out (1000 steps), followed by a MD of 250,000 steps but restraining only the enzyme's C$\alpha$ carbons. (3) All the system was relaxed again by 250,000 steps. (4) Finally, a 5 ns production MD was carried out for the protein, with and without ligand.

Because large conformational changes are not likely on inhibitor binding, the 5 ns were considered to be long enough simulation time. The simulated complex was held at constant temperature ($T$ = 310 K) and constant pressure ($P$ = 1 atm) with Langevin piston coupling algorithm.[22] Periodic boundary conditions were applied to the system in the three coordinate directions. An integration time step of 1 fs was used. The bonds involving hydrogen atoms were restrained by the SHAKE algorithm.[23]

The bonded and short-range interactions were calculated for every time step and for every third step for long-range electrostatic interactions. A cutoff value of 12 Å was used for the van der Waals and short-range electrostatic interactions. A switching function was enforced for the van der Waals forces to smoothen the cutoff. The water geometry was restrained rigid by using the SETTLE algorithm.[24] The simulations were conducted under the periodic boundary conditions with the full system, and long-range electrostatics were counted with the particle mesh Ewald method.[25]

The translocation pathway was evaluated using constant velocity SMD simulations on an equilibrated hMAO-A/5-HT (protonated and nonprotonated) complex and the corresponding cofactor inside of the protein. The SMD simulation was performed using as an initial structure a selected snapshot from the equilibration states in the MD simulations.

The force was applied through a connecting spring tethered at the center of mass of the ligands. A velocity of 0.0001 Å/time step and a harmonic constant of 6 kcal/(mol Å$^2$) were applied.

SMD simulations of all equilibrated systems spanned 2 ns. The direction of pulling was normalized between the so-called fixed and the SMD atoms. The fixed atom was positioned in the isoalloxazine ring of FAD and the SMD atom was obtained from the center mass of the ligand. Other directions were not investigated because the resultant pulling direction is guided according to the interactions arising from the passage of the substrate in the cavity from the isoalloxazine toward the entrance cavity of hMAO-A. Each simulation was repeated six times. All graphical analyses were performed using the VMD software.[26]

**p$K_a$ Calculations.** Residues able to uptake protons usually are glutamates[27] or histidines.[28] Because the p$K_a$ values of titratable groups in enzymes are shifted in many cases, and taking into account that these shifts can be critical for catalysis if the groups participate in proton transfer steps, evaluation of p$K_a$ values was carried out by means of PROPKA server (http://propka.ki.ku.dk/). This program is an accurate empirical method used to calculate p$K_a$.[29] Also as the level of p$K_a$ perturbation depends on the local environment of the respective residues; mean p$K_a$ values for selected residues were determined from an ensemble of structures collected from the 5 ns MD production step.

## RESULTS AND DISCUSSION

**5-HT Steered Molecular Dynamics Simulations.** In order to explore the binding and unbinding properties of 5-HT (protonated and deprotonated) in its pathway through the tunnel from the active site to the bulk, SMD simulations were considered.

The lowest potential energy conformation obtained from MD was used for SMD simulations, provided that the temperature and the total energy of the system had attained a constant value (fluctuations less than 5%). Also, the backbone root-mean-square deviations (rmsd) from the starting structures reached stable values. Then 5-HT (neutral and deprotonated) was pulled out from the active site applying at a constant velocity. The center mass is attached to a dummy atom via a virtual spring. This dummy atom is moved at constant velocity, and then the force between both is measured. The spring constant was 6 kcal/(mol Å$^2$) at a velocity of 10 Å/ns for a period of 2 ns. Figure 2 shows the variation of the average

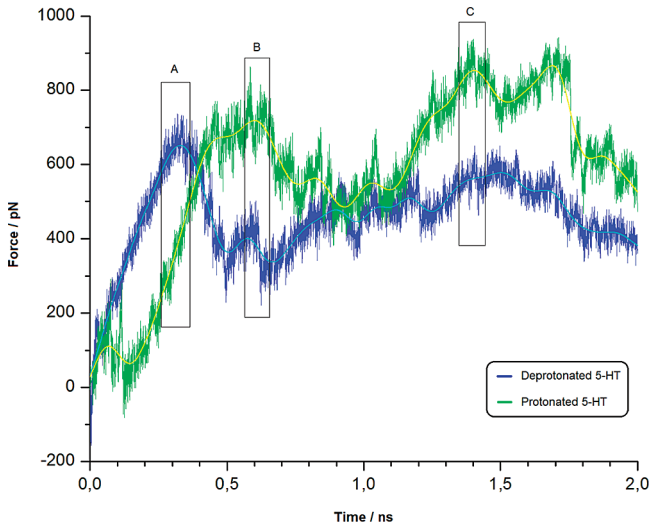


**Figure 2.** Steered molecular dynamics force profile for charged 5-HT (green) vs neutral 5-HT (blue). Points A, B, and C are local maxima force points along the pathway. The sharp drop observed in the force observed in ∼1.8 ns is where the substrate serotonin finds the bulk at the cavity entrance (site_1), so attractive interactions no longer exists.

force (from six independent simulations, in pN, see Figures SI1−SI2 of the Supporting Information) versus the simulation time (ns). Three main force peaks were found (denoted as A, B, and C) along a pathway from the active site to the entrance


dx.doi.org/10.1021/ci300081w | J. Chem. Inf. Model. 2012, 52, 1213−1221

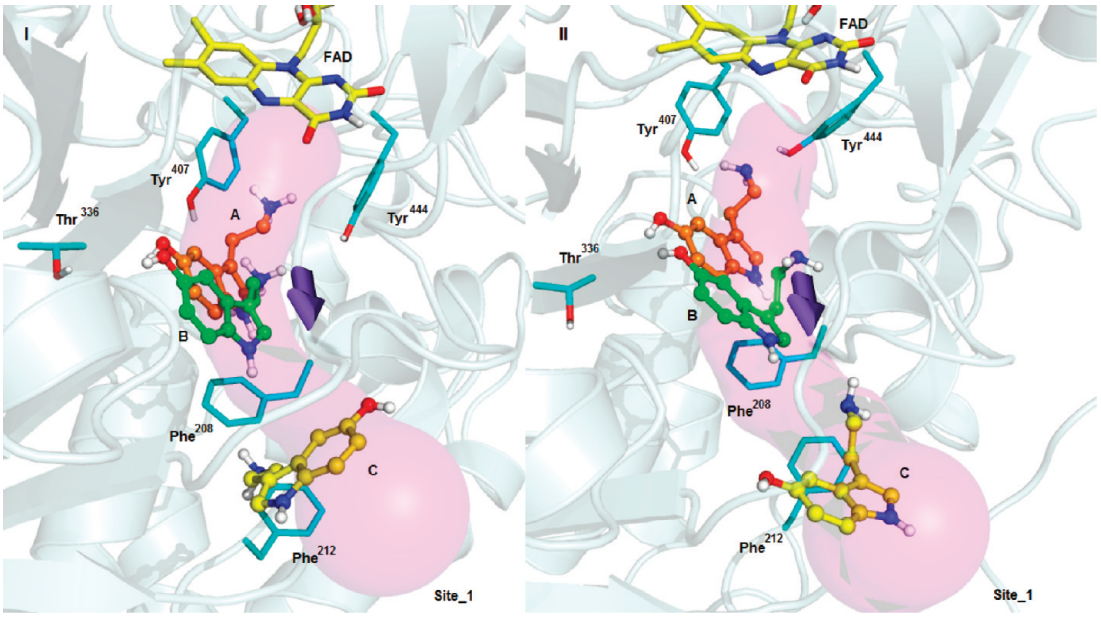


**Figure 3.** Steered molecular dynamic simulation extracted structures for protonated (I) and neutral serotonin (5-HT) species (II). 5-HT orange (A), green (B), and yellow (C) correspond to snapshots at 0.3, 0.6, and 1.4 ns of SMD, respectively. Purple arrows indicate SMD prospective direction of pulling from the active site to protein surface (pink path).

cavity as described by Son et al.[11] These peaks are related to the disruption of stable interactions between the substrate (protonanted and deprotonated) and several residues, as the substrate is being pulled. Although the force profiles for both neutral and protonated 5-HT are essentially comparable, it should be noticed that an important difference lies in the protonation state. Analysis of both profiles revealed different stages for the unbinding processes. Snapshots illustrating these processes are shown in Figure 3. As 5-HT passes through the active site to the cavity entrance,[11] both simulations generate H-bond interactions with $Thr^{336}$ in the active site; however, only the neutral substrate generates a H-bond with $Tyr^{444}$, leading to a peak at 0.3 ns (snapshot A). This result is in agreement with the accepted suggestion that the substrate arrives to the active site in its neutral state. Also, a $\pi$-stacking interaction is observed with $Phe^{208}$ that is not observed for the protonated state. As the substrate proceeds toward the entrance cavity, the same interactions are present for both states of the substrate 5-HT (peak at 0.6 ns, snapshot B), but from Figure 2, it can be noticed that only the protonated state evidence an increased passing force. This increased force could be the result of a hydrogen bond interaction between the N1 indolic proton of 5-HT and the carbonyl oxygen of $Phe^{208}$.

Unlike the above points A and B, no H-bonds are observed in snapshot C (peak at 1.4 ns), but a $\pi$-cation interaction between the charged substrate and $Phe^{112}$ is observed. This interaction is not present in the SMD simulation for the neutral substrate.

After the 1.8 ns simulation, the substrate has already crossed the cavity entrance and emerges into the aqueous bulk solution where it becomes completely surrounded by water molecules, as is noticed by the sharp drop in force for the protonated serotonin.

The starting point for the unbinding process for both neutral and protonated 5-HT at the active site differs mainly from the presence of H-bond interactions between neutral 5-HT and $Tyr^{444}$, where the pulling force for the neutral specie is about 650 pN compared to 350 pN for its protonated form. Once the molecules are located at the entrance cavity, a $\pi$-cation interaction of the protonated 5-HT with $Phe^{208}$ is established. As a consequence, the disruption of this interaction at 1.4 ns (snapshot C) requires a pulling force of about 900 pN, a larger value compared to the force required for the neutral species (about 500 pN). A second difference is the absence of basic residues lining the entire pathway. The charged amine group gradually breaks loose from the strong interactions with $Phe^{208}$, leaving the enzyme and plunging into the bulk aqueous medium after 1.4 ns (snapshot C). Both 5-HT species are completely pulled out of the enzyme into the aqueous solution after 2 ns. A comparison of the force profiles (Figure 2) may shed light on the relative interaction capacities of both neutral and protonated 5-HT forms. The higher number of stronger interactions for the neutral form with various side chains of hMAO-A residues should lead to a larger value for the external work required to pull the substrate out of the active site enzyme pocket. This larger work value may be related with the free energy difference associated with the process and ultimately with the greater affinity of the neutral species, in agreement with the proposed mechanism associated with substrate conversion.[30]

**Multigrid Docking and p$K_a$ Calculations.** Because of the deprotonated form **demonstrating** higher resistance in passage toward the bulk and therefore a higher driving force to disrupt interactions along a selected path, multigrid dockings of substrate in both forms (protonated and deprotonated) was carried out with the aim to seek for the plausible sites of deprotonation at the protein surface. Once these sites were found, p$K_a$ calculations were carried out to discriminate which residue(s) would be responsible for substrate deprotonation at the enzyme surface.

On the basis of the docking scores obtained by our multigrid docking procedure using AutoDock3.0.5, four spots on the enzyme surface can be considered as possible entrances or "anchorage" sites for both neutral or protonated forms of the substrate 5-HT. The final spot selection was based on the

analysis of residues able to capture protons, such as glutamates, aspartates, and histidines, provided that at physiological pH they may vary their p$K_a$ values. According to these criteria, two sites bear these aminoacids, the first, *site_1*, has a histidine, an aspartic, and a glutamic acid, meanwhile the second site, *site_2*, bear two glutamates and three aspartic acids. The latter site displayed a highly ionic character due to the presence of a cluster of negatively charge residues that eventually could guide the substrate from the bulk solvent to the enzyme's surface for its subsequent deprotonation.

From all the residues present in these two sites, only four displayed some changes in their p$K_a$ values: $Asp^{132}$, $Asp^{328}$, $His^{488}$, and $Glu^{327}$ (Table 1). The listed values correspond to p$K_a$ changes due to movements detected by molecular dynamics simulations observed in the 5 ns. From them, only two change their p$K_a$ values in more than 1.0 unit, i.e., $Glu^{327}$ (1.1 p$K_a$ unit) and $His^{488}$ (1.0 p$K_a$ unit). However, despite this change, only $Glu^{327}$ becomes the residue most likely to be found in its protonated form, i.e., increasing its ability to capture protons, being in fact the residue with a more basic profile when compared to the other residues (Table 1). This p$K_a$ change prompts this residue to be the best candidate to deprotonate substrates or inhibitors. It is worth noting that although the $Asp^{328}$ side chain is too acidic to uptake a proton, it might accomplish an important role as part of the environment, turning $Glu^{327}$ more basic according to observation by Sanderg et al.[31]

**Table 1. p$K_a$ Values of Residues in "Anchorage" Sites, Site_1 and Site_2, according to PROPKA Calculations**

| Residue | [a] p$K_{a,model}$ | [b] p$K_{a,PROPKA}$ | [c] $\Delta$p$K_a$ |
|---|---|---|---|
| $Asp^{132}$ | 3.8 | 3.8 ± 0.5 | 0 |
| $Asp^{328}$ | 3.8 | 3.5 ± 0.6 | 0.3 |
| $Glu^{327}$ | 4.5 | 5.6 ± 0.6 | 1.1 |
| $His^{488}$ | 6.5 | 5.5 ± 0.4 | 1 |

[a] p$K_a$ standard used by PROPKA for p$K_a$ calculations. [b] p$K_a$ calculated by PROPKA. [c] $\Delta pK_a = pKa_{model} - pKa_{PROPKA}$

Using an ensemble of snapshots obtained by 5 ns of MD, the CAVER program[32,33] (Figure 4) was used to determine if the proposed entrance sites are connected all the way through the catalytic site. The two sites were connected during all the dynamic simulation. On one hand, site_1, lined by residues such as $Glu^{492}$, $His^{488}$, and $Asp^{132}$ is nearby to the substrate entrance proposed by Son et al.,[11] which is surrounded by residues $Val^{93}$–$Glu^{95}$, $Tyr^{109}$–$Pro^{112}$, and $Phe^{208}$–$Asn^{212}$. On the other hand, site_2 is lined by a cluster of acidic residues such as $Glu^{185}$, $Glu^{327}$, $Asp^{328}$, $Glu^{329}$, and $His^{187}$. To the best of our knowledge, these sites have not yet been proposed as possible deprotonation sites for hMAO-A. It is worth noting that both entrance cavities are located near the C-terminal h-MAOA anchoring to the membrane surface (Figure 4).

Our results are in agreement with those stating that hMAO-A exhibits pH-dependent behavior according to steady-state kinetic studies carried out by Dunn et al.[10] According to these studies, a group in the enzyme–benzylamine complex is deprotonated for catalytic efficiency. Also, two distinct deprotonation steps were identified influencing catalytic activity with the increase and subsequent decrease in the enzyme-catalyzed reaction with an increasing pH, concluding that deprotonation of the amine moiety is required for catalysis. Also, a recent study carried out by Wang et al.[34] involving the effects of substituents of benzylamine analogues on the p$K_a$ of the ES complexes in human and rat

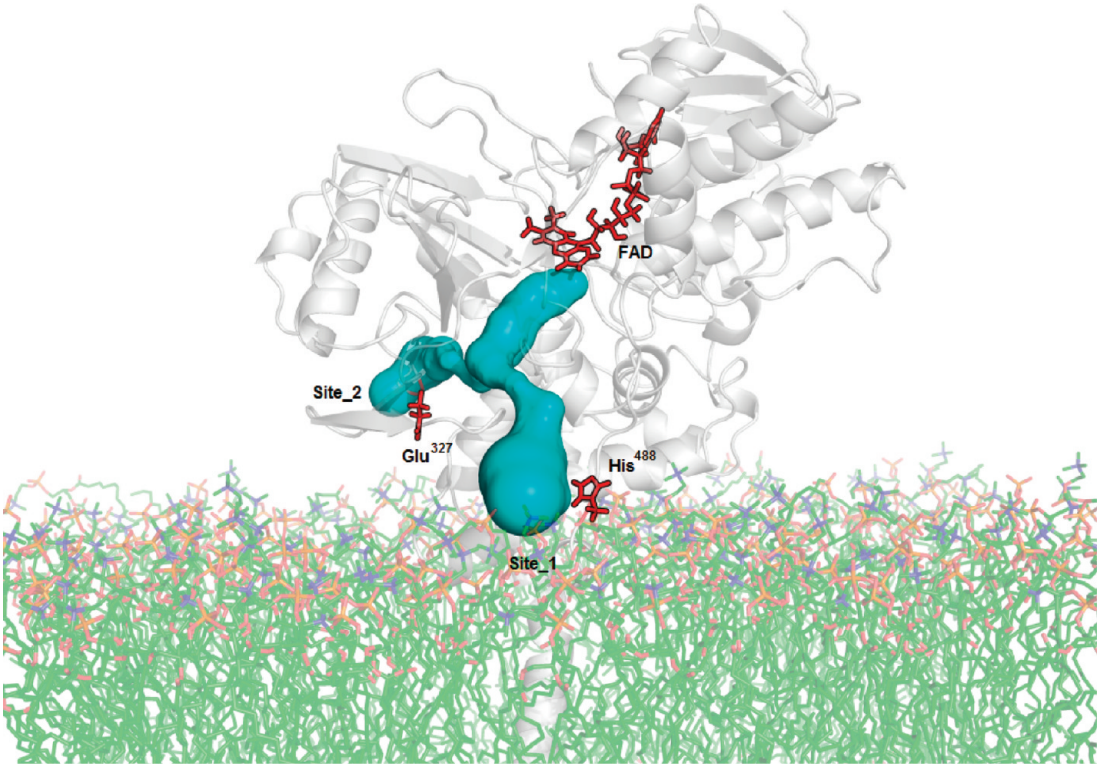


**Figure 4.** Site_1 and site_2 tunnels connected to the active site of hMAO-A obtained by CAVER using an ensemble of molecular dynamic snapshots. Cavities are shown in cyan, FAD (in the active site) and residues belonging to both cavities, i.e., $Glu^{327}$ and $His^{488}$ are shown in red sticks. The enzyme was inserted into the mitochondrial outer membrane according to the Son et al. description.[11].


dx.doi.org/10.1021/ci300081w | J. Chem. Inf. Model. 2012, 52, 1213–1221

MAO-A indicated that the perturbation of the macroscopic p$K_a$ (by ∼2 p$K$ units) reveal a deprotonation step of the ES complex in an initial binding of the protonated amine substrate prior to the chemical steps in catalysis. In this study the p$K_a$ values of the E and ES complexes of human and rat MAO A are found to be ∼8. As stated by the authors, the detailed molecular basis for this deprotonation step is missing. However, according to our modeling results, the identification of hMAO-A residues (vide supra) at two different loci on the enzyme's surface could be important in neutral and protonated substrate interactions and should assist further experimental work in order to corroborate these predictions because our findings provide a theoretical frame at the molecular level according to the interactions observed.

**Substrate Docking at the Active Site.** The tabulated results in Table 2 show the lowest docking energies for the protonated and deprotonated forms of 5-HT both in the active site and in the two proposed "anchorage" sites. The energy differences did not overcome 0.5 kcal mol$^{-1}$.

**Table 2. Docking Results for Substrate 5-HT. Lower Energy Pose in Its Protonated and Deprotonated Forms**

| | Lowest Energy pose [kcal*mol$^{-1}$] | |
|---|---|---|
| Site | Protonated | Deprotonated |
| Active Site | −9.46 | −9.38 |
| Site_1 | −9.89 | −9.39 |
| Site_2 | −10.67 | −10.18 |

Despite the similarity of the lowest energies of 5-HT at the active site, the protonated form displays hydrogen bonds and $\pi$-cation interactions with the backbone CO of Phe$^{208}$ that bear no relation with FAD nor the proposed oxidative deamination mechanism by Edmondson et al.[30] However, the neutral form displayed a better accommodation of the amine group toward the flavin moiety and the formation of a $\pi$-stacking interaction of the pyrrole group with Tyr$^{407}$ and Tyr$^{444}$ (Figure 5), which in turn seems to be an ideal position in order to achieve a functional substrate−enzyme complex.

**Inhibitor Dockings at the Active and "Anchorage" Sites.** To assess the nature of the ligand−receptor interactions and to investigate the protonation influence on the inhibitors, we carried out docking experiments into the active site of hMAO-A. The results are shown in Table 3. Prior to docking the inhibitors, the reliability of the docking method was tested redocking the inhibitor Harmine into the crystal structure of MAO-A.[11] The lowest-energy docking for this inhibitor matched the crystal position ($\alpha$-carbon rmsd 1.0 Å).

All inhibitors were docked at the same region within a hydrophobic site formed by Tyr$^{69}$, Asn$^{181}$, Phe$^{208}$, Val$^{210}$, Gln$^{215}$, Cys$^{323}$, Ile$^{325}$, Ile$^{335}$, Leu$^{337}$, Phe$^{352}$, Tyr$^{407}$, and Tyr$^{444}$ amino acid residues (Figure 6). These inhibitors reproduce the interactions observed for Harmine in the active site. When protonated, almost all compounds present higher docking energies at the protein surface (site_1 and site_2) than at the active site, although the differences compared to the deprotonated forms are small. Despite the fact that all reported inhibition potencies for amphetamine-based inhibitors evaluated on rat MAO-A and

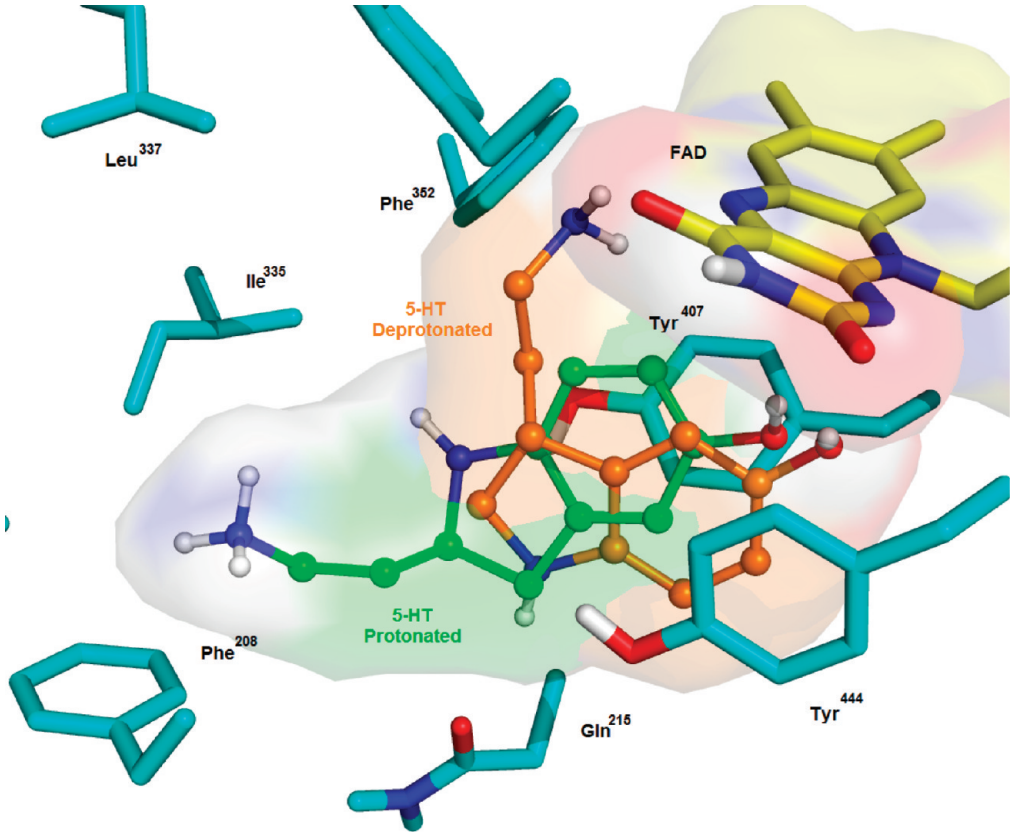


**Figure 5.** Conformation of 5-HT in the active site of hMAO-A. Amino acids are shown as cyan sticks. FAD located in the active site is shown as yellow sticks. The residues are numbered according to hMAO-A (PDB ID code 2Z5X). Deprotonated 5-HT is shown in orange, and protonated 5-HT is shown in green. Nitrogen and oxygen atoms are shown in blue and red, respectively.

**Table 3. $IC_{50}$ Values for Inhibitors and Lowest Energy Pose for Their Protonated and Deprotonated Forms[a]**

| Compound | $IC_{50}$ ($\mu$M) | Site | Lowest Energy pose (kcal mol$^{-1}$) | |
|---|---|---|---|---|
| | | | Protonated | Deprotonated |
| ETA | 0.1 | Active Site | −10.66 | −10.21 |
| | | Site_1 | −10.29 | −10.11 |
| | | Site_2 | −10.65 | −9.99 |
| MTA | 0.2 | Active Site | −9.78 | −9.38 |
| | | Site_1 | −9.22 | −9.07 |
| | | Site_2 | −9.78 | −9.19 |
| ALEPH2 | 3.2 | Active Site | −11.77 | −11.4 |
| | | Site_1 | −11.82 | −11.4 |
| | | Site_2 | −11.89 | −11.7 |
| MDA | 9.3 | Active Site | −10.67 | −9.88 |
| | | Site_1 | −8.93 | −8.65 |
| | | Site_2 | −10.04 | −10.58 |
| DOM | 24 | Active Site | −10.74 | −10.13 |
| | | Site_1 | −10.81 | −10.56 |
| | | Site_2 | −11.24 | −10.88 |
| DOI | 43 | Active Site | −11.09 | −10.44 |
| | | Site_1 | −11.36 | −11.07 |
| | | Site_2 | −11.42 | −11.25 |
| 2,5-DMA | >100 | Active Site | −10.67 | −10.19 |
| | | Site_1 | −10.2 | −9.89 |
| | | Site_2 | −11.69 | −10.91 |
| TMA | N.E. | Active Site | −10.69 | −9.64 |
| | | Site_1 | −10.13 | −9.87 |
| | | Site_2 | −10.77 | −10.01 |

[a]Compounds are listed in ascending order of $IC_{50}$ values.

active sites between rat and human are rather similar,[11] we used these pharmacological data to simplify our docking analysis. Two groups were formed according to their $IC_{50}$ values, namely, group A ($0.1 < IC_{50} < 9.3$ $\mu$M) and group B ($24 < IC_{50} < 100$ $\mu$M). TMA was considered separately because it shows no enzymatic activity at all.[2] It is worth noting that docking scores in Table 3 are similar for both protonation states of inhibitors, showing no correlation with the $IC_{50}$ values; however, the docking poses obtained allow us to extract some common features within the groups described above.

All inhibitors in group A display H-bonds between their amino group and the carbonyl group of residues Gln$^{215}$, Asn$^{182}$, and Tyr$^{444}$. As described above, these inhibitors achieved $\pi-\pi$ interactions between the carbonyl group of Gln$^{215}$ and the aromatic ring as Harmine.[11] Also, the *para* substituents of these inhibitors display a larger hydrophobic contact surface with the hydrophobic pocket, where the alkylthio moiety interacts with Phe$^{208}$, forming an aromatic sulfur interaction as described by Reid et al.[35] In contrast, group B, in spite of posing in the amine group nearby with the same carbonyl moieties, is displaced toward the carbonyl at C4 of the flavin ring. It is possible to argue that group B is marginally smaller in size than group A, which might diminish the contact surface at the substrate/inhibitor cavity.

All inhibitors superimpose their protonated and deprotonated amine moiety in the cavity, supporting the idea that the charged state in which the inhibitors find themselves is irrelevant when it comes to a preferred docking pose in the substrate/inhibitor cavity. Moreover, the marginal energy differences obtained in their docking poses do not allow us to conclude if

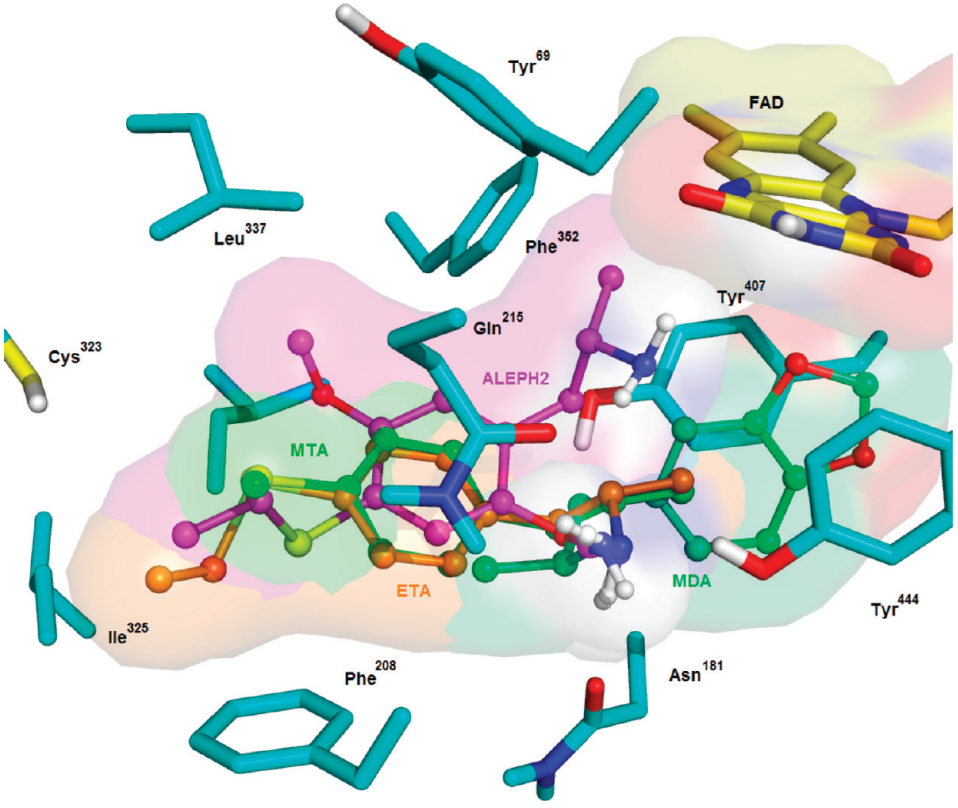


**Figure 6.** Group A of inhibitors docked in the inhibitor cavity of hMAO-A. The residues are numbered according to hMAO-A(PDB ID code 2Z5X) . Inhibitors are colored as follows: orange, ETA; green, MTA; light green, MDA; and purple, ALEPH-2. Nitrogen and oxygen atoms are shown in blue and red, respectively, and the sulfur atom is shown in yellow.


dx.doi.org/10.1021/ci300081w | J. Chem. Inf. Model. 2012, 52, 1213−1221

the protonated state is preferred by the inhibitors to reach the active site cavity. Indeed, no data regarding the path used to access the active site have been published yet.

Interestingly, TMA displays two different docking poses according to its protonation state, which may imply an increased mobility upon docking at the active site. One might speculate about the possibility that inhibitors might possess low mobility to block the active site or the entrance of substrate so the lack of conformational restriction may be associated with lack of pharmacological activity.

Our docking results allow us to conclude that inhibition is favored if the inhibitors prefer specific orientations associated with their structural features, such as the interaction of the amine group with $Gln^{215}$, $Asn^{182}$, and $Tyr^{444}$; the $\pi-\pi$ interaction between the carbonyl group of $Gln^{215}$; and the side chains of these inhibitors at the *p*-position interacting with a larger area in the hydrophobic pocket.

Finally, comparison of the results obtained with the more potent ethylthioamphetamine derivatives with respect to 5-HT shows the importance of a favored docking pose and the interaction of these inhibitors with some aromatic residues in a corresponding aromatic cage of hMAO-A.

## CONCLUSIONS

Our results support the hypothesis that both 5-HT and inhibitors reach the hMAO-A surface in their protonated forms that enable them to interact with the "anchorage" sites described (i.e., site_1 and site_2), where they can be deprotonated in situ by specific basic amino acid residues for later access to the active/inhibition site. Nevertheless, when the active site is reached, the specific interactions of substrate and inhibitors seem differ, possibly associated with differential interaction abilities of the deprotonated species of substrate or inhibitors.

Steered molecular dynamics confirm the latter finding, as on its way toward the entrance cavity and into the aqueous bulk solution, the neutral substrate interacts with $Tyr^{444}$, $Thr^{336}$, and $Phe^{208}$, whereas protonated 5-HT interacts additionally with $Phe^{112}$. On one hand, neutral 5-HT makes a H-bond with $Tyr^{444}$, leading to larger required work to pull the substrate from the active site cavity in comparison with protonated 5-HT. The increased value of the force of the charged 5-HT at the cavity entrance may provide additional stability for this specie outside where it can be deprotonated by other groups. Thus, SMD calculations suggests that the protonated substrate form as the preferred specie to interact with some residues in specific locations on the surface of the protein, but the neutral substrate form the preferred specie upon interacting with the active site. Thus, an alternation between protonation and deprotonation might be required for proper access to the active site of hMAO-A.

## ASSOCIATED CONTENT

### Supporting Information

**SI1**: Six independent SMD simulations for protonated 5-HT (Force (pN) versus simulation time (ns)) used to calculate the variation of the average force shown in Figure 2. **SI2**: Six independent SMD simulations for deprotonated 5-HT (Force (pN) versus simulation time (ns)) used to calculate the variation of the average force shown in Figure 2. This information is available free of charge via the Internet at http://pubs.acs.org

## AUTHOR INFORMATION

### Corresponding Author

*E-mail: gzapata@uchile.cl. Telephone:56-2-9782843.

### Notes

The authors declare no competing financial interest.

## ACKNOWLEDGMENTS

This work was supported by Fondo Nacional de Desarrollo Científico y Tecnológico FONDECYT, Grants N° 1090215 and N° 11085002, PDA-23. G.A.Z.T. acknowledges Programa U-APOYA Línea 1, Vicerrectoría de Investigación y Desarrollo, Universidad de Chile.

## REFERENCES

(1) Youdim, M. B. H.; Edmonson, D.; Tipton, K. F. The therapeutic potential of monoamine oxidase inhibitors. *Nat. Rev. Neurosci.* **2006**, *7*, 295−309.

(2) Scorza, M. C.; Carrau, C.; Silveira, R.; Zapata-Torres, G.; Cassels, B. K.; Reyes-Parada, M. Monoamine oxidase inhibitory properties of some methoxylated and alkylthio amphetamine derivatives. Structure−activity relationships. *Biochem. Pharmacol.* **1997**, *54*, 1361−1369.

(3) Gnerre, C.; Catto, M.; Leonetti, F.; Weber, P.; Carrupt, P. A.; Altomare, C.; Carotti, A.; Testa, B. J. Inhibition of monoamine oxidases by functionalized coumarin derivatives: Biological activities, QSARs, and 3D-QSARs. *J. Med. Chem.* **2000**, *43*, 4747−4758.

(4) Chimenti, F.; Fioravanti, R.; Bolasco, A.; Chimenti, P.; Secci, D.; Rossi, F.; Yáñez, M; Orallo, F.; Ortuso, F.; Alcaro, S. Chalcones: A valid scaffold for monoamine oxidases Inhibitors. *J. Med. Chem.* **2009**, *52*, 2818−2824.

(5) Zisook., S. E. A clinical overview of monoamine oxidase inhibitors. *Psychosomatics* **1985**, *26*, 240−251.

(6) Fernández, H. H.; Chen, J. J. Monoamine oxidase-B inhibition in the treatment of Parkinson's disease. *Pharmacotherapy* **1985**, *27*, 174−185.

(7) Lühr, S.; Vilches-Herrera, M.; Fierro, A.; Ramsay, R. R.; Edmondson, D. E.; Reyes-Parada, M.; Cassels, B. K.; Iturriaga-Vásquez, P. 2-Arylthiomorpholine derivatives as potent and selective monoamine oxidase B inhibitors. *Bioorg. Med. Chem.* **2010**, *18*, 1388−1395.

(8) Pratuangdejkul, J.; Nosoongnoen, W.; Guérin, G. A.; Loric, S.; Conti, M.; Launay, J. M.; Manivet, P. Conformational dependence of serotonin theoretical pKa prediction. *Chem. Phys. Lett.* **2006**, *420*, 538−544.

(9) Jones, T. Z. E.; Balsa, D.; Unzeta, M.; Ramsay, R. R. Variations in activity and inhibition with pH: The protonated amine is the substrate for monoamine oxidase, but uncharged inhibitors bind better. *J. Neural Transm.* **2007**, *114*, 707−712.

(10) Dunn, R. V.; Marshall, K. R.; Munro, A. W.; Scrutton, S. N. The pH dependence of kinetic isotope effects in monoamine oxidase A indicates stabilization of the neutral amine in the enzyme−substrate complex. *FEBS J.* **2008**, *275*, 3850−3858.

(11) Son, S. Y.; Yoshimura, M. J.; Tsukihara, T. Structure of human monoamine oxidase A at 2.2-Å resolution. The control of opening the entry for substrates/inhibitors. *Proc. Natl. Acad. Sci. U.S.A.* **2008**, *105*, 5739−5744.

(12) Ma, J.; Yoshimura, M.; Yamashita., E.; Nakagawa, A.; Ito, A.; Tsukihara, T. Structure of rat monoamine oxidase a and its specific recognitions for substrates and inhibitors. *J. Mol. Biol.* **2004**, *338*, 103−114.

(13) Das, N.; Dash, B.; Dhanawat, M.; Shrivastava, S. K. Design, synthesis, preliminary pharmacological evaluation, and docking studies of pyrazoline derivatives. *Chem. Pap.* **2012**, *66*, 67−74.

(14) Cerqueira, E. C.; Netz, P. A.; Diniz, C.; do Canto, V. P.; Follmer, C. Molecular insights into human monoamine oxidase (MAO) inhibition by 1,4-naphthoquinone: Evidences for menadione (vitamin K3) acting as a competitive and reversible inhibitor of MAO. *Bioorg. Med. Chem.* **2011**, *19*, 7416−7424.

(15) Gordon, J. C.; Myers, J. B.; Folta, T.; Shoja, V.; Heath, L. S.; Onufriev, A. H++: A server for estimating pKas and adding missing hydrogens to macromolecules. *Nucleic Acids Res.* **2005**, *33*, 368−371.
(16) Frisch, M. J.; Trucks, G. W.; Schlegel, H. B.; Scuseria; G. E.; Robb; M. A.; Cheeseman, J. R.; Montgomery, J. A. Jr; Vreven, T.; Kudin, K. N.; Burant, J. C.; Millam, J. M.; Iyengar, S. S.; Tomasi, J.; Barone, V.; Mennucci, B.; Cossi; M.; Scalmani, G.; Rega, N.; Petersson, G. A.; Nakatsuji, H.; Hada, M.; Ehara, M.; Toyota, K.; Fukuda, R.; Hasegawa, J.; Ishida, M.; Nakajima, T.; Honda, Y.; Kitao, O.; Nakai, H.; Klene, M.; Li, X.; Knox, J. E.; Hratchian, H. P.; Cross, J. B.; Bakken, V.; Adamo, C.; Jaramillo, J.; Gomperts, R.; Stratmann, R. E.; Yazyev, O.; Austin, A. J.; Cammi, R.; Pomelli, C.; Ochterski, J. W.; Ayala, P. Y.; Morokuma, K.; Voth, G. A.; Salvador, P.; Dannenberg, J. J.; Zakrzewski, V. G.; Dapprich, S.; Daniels, A. D.; Strain; M. C.; Farkas, O.; Malick, D. K.; Rabuck, A. D.; Raghavachari, K.; Foresman, J. B.; Ortiz; J. V.; Cui, Q.; Baboul, A. G.; Clifford, S.; Cioslowski, J.; Stefanov, B. B.; Liu, G.; Liashenko, A.; Piskorz, P.; Komaromi, I.; Martin, R. L.; Fox, D. J.; Keith, T.; Al-Laham, M. A; Peng, C. Y.; Nanayakkara, A.; Challacombe, M.; Gill, P. M. W.; Johnson, B.; Chen, W.; Wong, M. W.; Gonzalez, C.; Pople, J. A. *Gaussian 98*, Revision A.9; Gaussian, Inc.: Pittsburgh, PA, 2001.
(17) Morris, G. M.; Goodsell, D. S.; Halliday, R. S.; Huey, R.; Hart, W. E.; Belew, R. K.; Olson, A. J. Automated docking using a Lamarckian genetic algorithm and empirical binding free energy function. *J. Comput. Chem.* **1998**, *19*, 1639−1662.
(18) Phillips, J. C.; Braun, R.; Wang, W.; Gumbart, J.; Tajkhorshid, E.; Villa, E.; Chipot, C.; Skeel, R. D.; Kale, L.; Schulten, K. Scalable molecular dynamics with NAMD. *J. Comput. Chem.* **2005**, *26*, 1781−1802.
(19) MacKerell, A. D., Jr.; Bashford, D.; Bellott, M.; Dunbrack, R. L., Jr.; Evanseck, J. D.; Field, M. J.; Fischer, S.; Gao, H. J.; Guo, H.; Ha, S.; Joseph-McCarthy, D.; Kuchnir, L.; Kuczera, K.; Lau, F. T. K.; Mattos, C.; Michnick, S.; Ngo, T.; Nguyen, D. T.; Prodhom, B.; Reiher, W. E., III; Roux, B.; Schlenkrich, M.; Smith, J. C.; Stote, R.; Straub, J.; Watanabe, M.; Wiórkiewicz-Kuczera, J.; Yin, D.; Karplus, M. All-atom empirical potential for molecular modeling and dynamics studies of proteins. *J. Phys. Chem. B* **1998**, *102*, 3586−3616.
(20) Beglov, D.; Roux, B. Finite representation of an infinite bulk system, solvent boundary potential for computer simulations. *J. Chem. Phys.* **1994**, *100*, 9050−9063.
(21) Wang, J.; Wolf, R. M.; Caldwell, J. W.; Kollman, P. A.; Case, D. A. Development and testing of a general AMBER force field. *J. Comput. Chem.* **2004**, *25*, 1157−1174.
(22) Feller, S. E.; Zhang, Y.; Pastor, R. W.; Brooks, B. R. Constant pressure molecular dynamics simulation: The Langevin piston method. *J. Chem. Phys.* **1995**, *103*, 4613−4621.
(23) Ryckaert, J.; Ciccotti, G.; Berendsen, H. J. Numerical integration of the Cartesian equations of motion of a system with constraints: Molecular dynamics of *n*-alkanes. *J. Comput. Phys.* **1977**, *23*, 327−341.
(24) Pak, S. M. SETTLE: An analytical version of the SHAKE and RATTLE algorithm for rigid water models. *J. Comput. Chem.* **1992**, *13*, 952−962.
(25) Darden, T.; York, D.; Pedersen, L. Particle mesh Ewald: An Wlog(N) method for Ewald sums in large systems. *J. Chem. Phys.* **1993**, *98*, 10089−10092.
(26) Humphrey, W.; Dalke, A.; Schulten, K. VMD: Visual molecular dynamics. *J. Mol. Graphics* **1996**, *14*, 33−38.
(27) Seibold, S. A.; Mills, D. A.; Ferguson-Miller, S.; Cukier, R. I. Water chain formation and possible proton pumping routes in *Rhodobacter sphaeroides* cytochrome c oxidase: A molecular dynamics comparison of the wild type and R481K mutant. *Biochemistry* **2005**, *44*, 10475−10485.
(28) Deonarain, M. P.; Berry, A.; Scrutton, N. S.; Perham, R. N. Alternative proton donors acceptors in the catalytic mechanism of the glutathione-reductase of *Escherichia coli*: The role of histidine-439 and tyrosine-99. *Biochemistry* **1989**, *28*, 9602−9607.
(29) Adam, C. L.; Crippen, G. M. Predicting pKa. *J. Chem. Inf. Model.* **2009**, *49*, 2013−2033.
(30) Edmondson, D. E.; Mattevi, A; Binda, C.; Li, M.; Hubálek, F. Structure and mechanism of monoamine oxidase. *Curr. Med. Chem.* **2004**, *11*, 1983−1993.
(31) Sandberg, L.; Edholm, O. pKa calculations along a bacteriorhodopsin trajectory. *Biophys. Chem.* **1997**, *65*, 189−204.
(32) Petřek, M.; Otyepka, M.; Banáš, P.; Košinová, P.; Koča, J.; Damborský, J. CAVER: A new tool to explore routes from protein clefts, pockets and cavities. *BMC Bioinf.* **2006**, *7*, 316−324.
(33) Damborský, J; Petrek, M; Banáš, P; Otyepka, M. Identification of tunnels in proteins, nucleic acids, inorganic materials and molecular ensembles. *Biotechnol. J.* **2007**, *2*, 62−67.
(34) Wang, J.; Edmondson, D. E. 2H kinetic isotope effects and pH dependence of catalysis as mechanistic probes of rat monoamine oxidase A: Comparisons with the human enzyme. *Biochemistry* **2011**, *50*, 7710−7717.
(35) Reid, K. S. C.; Lindley, P. F.; Thornton, J. M. Sulphur-aromatic interactions in proteins. *FEBS Lett.* **1985**, *190*, 209−213.